

# Three dimensional application of the Complementary Mild-Slope Equation

Yaron Toledo and Yehuda Agnon

*Civil and Environmental Engineering, Technion, Haifa, Israel.*

---

## Abstract

The Complementary Mild-Slope Equation (CMSE) is a depth-integrated equation, which models refraction and diffraction of linear time-harmonic water waves. For 2D problems, it was shown to give better agreements with exact linear theory compared to other mild-slope (MS) type equations. However, no reference was given to 3D problems. In contrast to other MS-type models, the CMSE is derived in terms of a stream-function vector rather than in terms of a velocity potential. For the 3D case, this complicates the governing equation and creates difficulties in formulating an adequate number of boundary conditions. In this paper, the CMSE is re-derived from Hamilton's principle using the Irrotational Green-Naghdi equations with a correction for the 3D case. A parabolic version of it is presented as well. The additional boundary conditions needed for 3D problems are constructed using the irrotationality condition. The CMSE is compared with an accurate numerical model and wave tank experiments for 3D problems. The results show very good agreement.

*Key words:* **mild-slope equation, linear waves, stream function formulation, coastal and offshore engineering.**

---

## 1 Introduction

The Mild-Slope Equation (MSE), presented by Berkhoff [1], assumed, as implied by its name, a mild slope, in two different steps. The first is in the assumption of a vertical structure, which relates to horizontal bottom. The second is after averaging over the depth, where the second derivative of the bottom variation and the square of its gradient were neglected. The depth-averaging procedure allowed the elimination of the vertical coordinate in solving a refraction-diffraction wave problems.

Many works continued this pioneering derivation (see [2,3]). In particular, two known extensions are the Modified Mild-Slope Equation (MMSE) and the Extended Mild-Slope Equation (EMSE). While keeping the same vertical structure, the two equations improved the MSE in different ways. The MMSE presented by Chamberlain & Porter [4], took into account the higher bottom gradient  $\nabla^2 h$  and  $(\nabla h)^2$  that were neglected in the original derivation. Kirby's EMSE [5] assumed a constant mean bottom depth,  $h_0$ , together with a small amplitude of rapid variation,  $\delta$ , which applies mostly to the case of scattering due to bottom undulation, and the averaging over depth used Green's second identity.

Agnon [6] used operational calculus to derive the Augmented Mild-Slope Equation, which gives a wider perspective on the above equations. The AMSE is a fully accurate mild-slope (MS) type equation that consists of pseudo-differential operators. It can be approximated by a differential equation. The method of approximation, its order and the chosen small parameter construct an approximated equation. This allows to rigorously derive MS-type equations such as the MSE, MMSE and EMSE, with good understanding of their nature.

Unlike the above MS-type models, the CMSE, presented by Kim & Bai [7], is derived in terms of a stream-function vector rather than in terms of a velocity potential. This enables the vertical structure to satisfy exactly the kinematic boundary condition on the uneven bottom. In contrast, the velocity potential vertical structure assumption satisfies exactly the bottom boundary condition only in the horizontal bottom case. For 2D problems, the CMSE was shown to give better agreement with exact linear theory compared to other MS-type equations.

---

*Email address: yaront@tx.technion.ac.il, agnon@tx.technion.ac.il*  
(Yaron Toledo and Yehuda Agnon).

However, for the 3D case, the stream-function vector formulation complicates the governing equation by making it a 2D vector equation, rather than a scalar one, that in addition, contains mixed derivatives. It also creates difficulties in formulating an adequate number of boundary conditions as two boundary conditions are needed in each impermeable lateral boundary due to the 2D stream-function vector.

Using *Cosserat* surfaces, Green & Naghdi [8] developed an alternative approach for modeling incompressible fluid dynamic problems in their work on directed fluid sheets. Their approach, which was later referred to as the Green-Naghdi (GN) equations, can account for viscosity and rotationality. Kim, *et al.* [9] constructed an irrotational model based on the GN equations for irrotational and inviscid flows, which is referred to as the Irrotational Green-Naghdi (IGN) equations.

In this work, the CMSE is re-derived from Hamilton's principle using the IGN equations with a correction for the 3D case as is shown in Section 2. In Section 3, the needed additional boundary conditions are constructed using the irrotationality condition, and the mixed derivatives are being defined in terms of second order ones to yield a relation transforming the grad-div operator to a vector Laplacian one. A parabolic approximation is applied to the CMSE model in Section 4, and numerical results are presented in Section 5.

## 2 The Irrotational Green-Naghdi Equations

### 2.1 Constructing the equations of motion using the IGN Lagrangian

Let us define  $\Psi$  as a stream function vector

$$\Psi(\mathbf{x}, z, t) \equiv (\Psi^I, \Psi^{II}) \equiv \int_{-h}^z \mathbf{u}(x, \zeta) d\zeta, \quad \mathbf{u} = (u, v), \quad \mathbf{x} = (x, y), \quad (1)$$

where  $\mathbf{u}$  is the horizontal velocity vector and  $\mathbf{x}$  is the horizontal location vector. From equation (1) the velocity field is found from  $\Psi$  by:

$$\mathbf{u} = \frac{\partial \Psi}{\partial z}, \quad w = -\nabla \cdot \Psi. \quad (2)$$

The equations governing the irrotational flow of an incompressible inviscid fluid with a free surface over a horizontal bottom can be constructed using

the Irrotational Green-Naghdi Equations derived from Hamilton's principle, see Kim *et al.* [9,10]. The Lagrangian is given as

$$\mathbf{L} = \iint L dx dy,$$

$$\frac{1}{\rho}L = \phi (\eta_t + \nabla \cdot \Psi + \Psi_z \cdot \nabla \eta)_{z=\eta} + \frac{1}{2} \int_{-h}^{\eta} (|\Psi_z|^2 + |\nabla \cdot \Psi|^2) dz - \frac{1}{2} g \eta^2. \quad (3)$$

Here  $\nabla = \left( \frac{\partial}{\partial x}, \frac{\partial}{\partial y} \right)$ ,  $h = h(\mathbf{x})$  is the water depth,  $\eta = \eta(\mathbf{x}, t)$  is the surface elevation and  $\phi = \phi(\mathbf{x}, t)$  is a Lagrange multiplier function. The origin is on the undisturbed water level and  $z$  is positive upward.

Taking the first variation of the Lagrangian with respect to  $\phi$ ,  $\eta$  and  $\Psi$  gives three Euler-Lagrange equations:

$$\frac{\delta L}{\delta \Psi} : \quad \nabla(\nabla \cdot \Psi) + \Psi_{zz} = 0 \quad -h < z < \eta \quad (4)$$

$$\frac{\delta L}{\delta \eta} : \quad \phi_t + \frac{1}{2} (\Psi_z)^2 + \frac{1}{2} (\nabla \cdot \Psi)^2 + g\eta = 0 \quad z = \eta \quad (5)$$

$$\frac{\delta L}{\delta \phi} : \quad \eta_t + \nabla \cdot \Psi + \Psi_z \cdot \nabla \eta = 0 \quad z = \eta \quad (6)$$

By using this formulation, Kim & Bai [7] showed that the impermeable bottom boundary condition on  $z = -h(x, y)$  is satisfied exactly, and the definition of  $\Psi$  can be used to construct a Dirichlet boundary condition,

$$\Psi = 0 \quad z = -h. \quad (7)$$

This gives us the complete set of equations and boundary conditions that govern the irrotational flow of an incompressible inviscid fluid with a free surface. From equation (5), we can see that the Lagrange multiplier for the kinematic boundary condition on the free surface,  $\phi$ , is actually the velocity potential on the free surface as shown by Kim *et al.* [9].

## 2.2 Constructing the approximated Euler-Lagrange equations

Expanding equation (3) around  $z = 0$  using Taylor's expansion up to  $O((ka)^2)$  gives

$$\frac{1}{\rho}L = \phi (\eta_t + \nabla \cdot \Psi)_{z=0} + \frac{1}{2} \int_{-h}^0 (|\Psi_z|^2 + |\nabla \cdot \Psi|^2) dz - \frac{1}{2} g \eta^2 \quad (8)$$

In order to eliminate the  $z$ -coordinate and construct a MS-type equation a vertical profile will be assumed. The vertical profiles will be chosen as in the linear solution of the horizontal bottom problem as was done by Kim & Bai [7] :

$$\Psi(\mathbf{x}, z, t) = f(k, h, z) \Psi_0(\mathbf{x}, t), \quad f(k, h, z) = \frac{\sinh(k(h)(z+h))}{\sinh(k(h)h)}, \quad (9)$$

where  $k$  is the wave number function and the relation between  $k$  and  $h$  comes from the linear dispersion relation,  $\omega^2 = gk \tanh(kh)$ . Note that the vertical profile  $f$  forces  $\Psi$  to satisfy the bottom boundary condition (7) as it vanishes at  $z = -h$ . It is normalized to 1 at  $z = 0$ , making  $\Psi_0$  represent the stream function vector at the undisturbed water level. By substituting equation (9), the Lagrangian (8) becomes

$$\begin{aligned} \frac{1}{\rho} L = & \phi (\eta_t + \nabla \cdot \Psi_0) + \\ & + \frac{1}{2} \int_{-h}^0 \left( \left| \frac{\partial f}{\partial z} \Psi_0 \right|^2 + \left| \frac{\partial f}{\partial h} \nabla h \cdot \Psi_0 + f \nabla \cdot \Psi_0 \right|^2 \right) dz - \frac{1}{2} g \eta^2. \end{aligned} \quad (10)$$

The integral on the depth can be applied to the coefficients that contain  $f$  and its derivatives to give

$$\begin{aligned} \frac{1}{\rho} L = & \phi (\eta_t + \nabla \cdot \Psi_0) + \frac{1}{2} \bar{d} |\Psi_0|^2 + \text{Re} \{ b (\nabla h \cdot \Psi_0) \nabla \cdot \Psi_0^* \} + \\ & + \frac{1}{2} c |\nabla h \cdot \Psi_0|^2 + \frac{1}{2} \bar{a} |\nabla \cdot \Psi_0|^2 - \frac{1}{2} g \eta^2, \end{aligned} \quad (11)$$

where  $\bar{a}$ ,  $b$ ,  $c$  and  $\bar{d}$  are defined as

$$\begin{aligned} \bar{a}(h) &= \int_{-h}^0 f^2 dz, & b(h) &= \int_{-h}^0 f \frac{\partial f}{\partial h} dz, \\ c(h) &= \int_{-h}^0 \left( \frac{\partial f}{\partial h} \right)^2 dz, & \bar{d}(h) &= \int_{-h}^0 \left( \frac{\partial f}{\partial z} \right)^2 dz. \end{aligned}$$

Taking the first variation of the Lagrangian with respect to  $\phi$ ,  $\eta$  and  $\Psi$  gives us three Euler-Lagrange equations:

$$\frac{\delta L}{\delta \Psi} : -\nabla \phi + \bar{d} \Psi_0 - \nabla (\bar{a} (\nabla \cdot \Psi_0) + b (\nabla h \cdot \Psi_0)) +$$

$$+b(\nabla \cdot \Psi_0) \nabla h + c(\nabla h \cdot \Psi_0) \nabla h = 0 \quad (12)$$

$$\frac{\delta L}{\delta \eta} : \phi_t + g\eta = 0 \quad (13)$$

$$\frac{\delta L}{\delta \phi} : \eta_t + \nabla \cdot \Psi_0 = 0 \quad (14)$$

From equations (13) and (14), we find  $\phi$  as a function of  $\Psi_0$ ,

$$\phi_{tt} = g\nabla \cdot \Psi_0, \quad (15)$$

and then, by regarding the solution as harmonic in time, equation (15) becomes

$$\phi = -\frac{g}{\omega^2} \nabla \cdot \Psi_0. \quad (16)$$

$\Psi_0$  and  $\phi$  now represent only their harmonic amplitude and no longer change in time. Substituting equation (16) into (12) yields

$$-\nabla(a(\nabla \cdot \Psi_0) + b(\nabla h \cdot \Psi_0)) + (b\nabla \cdot \Psi_0 + c\nabla h \cdot \Psi_0) \nabla h - k(h)^2 a \Psi_0 = 0, \quad (17)$$

$$a(h) = \int_{-h}^0 f^2 dz - \frac{g}{\omega^2} = \frac{\coth(kh)}{2k} \left(1 + \frac{2kh}{\sinh(2kh)}\right) = -\frac{gk^2}{\omega^4} CC_g, \quad (18)$$

$$b(h) = \int_{-h}^0 f \frac{\partial f}{\partial h} dz = \frac{1}{4 \sinh^2(kh)} \frac{2kh \cosh(2kh) - \sinh(2kh)}{2kh + \sinh(2kh)}, \quad (19)$$

$$\begin{aligned} c(h) &= \int_{-h}^0 \left(\frac{\partial f}{\partial h}\right)^2 dz = \\ &= \frac{k}{12 \sinh^2(kh)} \frac{-12kh + 8(kh)^3 + 3 \sinh(4kh) + 12(kh)^2 \sinh(2kh)}{(2kh + \sinh(2kh))^2}. \end{aligned} \quad (20)$$

Here,  $\Psi_0 = \Psi(\mathbf{x})$  and the relation  $\bar{d}(h) = -k(h)^2 a$  was used for simplification. For further use, note that equations (18) and (19) yield the relation  $\nabla a = 2b\nabla h$ .

We can see that from the IGN Lagrangian we derived the same linear equation as Kim & Bai [7] did (i.e. the CMSE - complementary mild-slope equation) with one correction in the  $c$ -coefficient term as can be seen by comparing equation (17) and the CMSE as it was given by Kim & Bai [7]:

$$-\nabla(a(\nabla \cdot \Psi_0) + b(\nabla h \cdot \Psi_0)) + b\nabla \cdot \Psi_0 \nabla h + (-k(h)^2 a + c\nabla h \cdot \nabla h) \Psi_0 = 0. \quad (21)$$

The CMSE was also derived using the Lagrangian given by Kim & Bai [7] and yielded the same results as equation (17), thus correcting an error in their derivation. In the 2D case, for which they have presented numerical results, their equation coincides with the corrected equation.

### 3 The stream function representation in the 3D case

#### 3.1 The impermeable boundary condition

In the stream function formulation, a set of two coupled differential equations for  $\Psi_0^I$  and  $\Psi_0^{II}$  needs to be solved. This implies that boundary conditions are needed for both components. When regarding the impermeable boundary condition, for example, a wall at  $y = 0$ , the restriction  $v = 0$  together with the definition of  $\Psi$  (1) yields one boundary condition:

$$\Psi_0^{II} = 0. \quad (22)$$

The boundary condition for  $\Psi_0^I$  can be found using the irrotationality condition in the  $\hat{z}$  direction. Note that from the definition of  $\Psi$ , irrotationality is satisfied naturally in  $\hat{x}$  and  $\hat{y}$  directions, but not in the  $\hat{z}$  one. Using the horizontal irrotationality condition and the Leibnitz rule of differentiation of integrals we get

$$\begin{aligned} [\Psi_y^I - \Psi_x^{II}]_{z=0} &= \partial_y \int_{-h}^0 u dz - \partial_x \int_{-h}^0 v dz = \\ &= \int_{-h}^0 (u_y - v_x) dz + [h_y u - h_x v]_{z=-h} = \\ &= (h_y \Psi_0^I - h_x \Psi_0^{II}) \partial_z f|_{z=-h}. \end{aligned} \quad (23)$$

For the case of a wall at  $y = 0$ , equation (23) together with the boundary condition (22) yield a boundary condition for  $\Psi_0^I$ :

$$\partial_y \Psi_0^I = h_y \Psi_0^I \partial_z f|_{z=-h}, \quad (24)$$

where

$$\partial_z f|_{z=-h} = \frac{k(h)}{\sinh(k(h)h)} \quad (25)$$

Nevertheless, it is problematic to use the boundary condition given in (24) for the CMSE (17).  $\Psi_0^I$  is differentiated with respect to  $y$  only to the first order and the boundary condition (24) is appropriate for a second order differentiation. The derivatives with respect to  $y$  come as mixed derivatives  $\Psi_{xy}^I$  and  $\varphi_{xy}^I$  resulting from the grad-div operator. This operator  $(\nabla\nabla\cdot)$  can be transformed into the vector Laplace operator  $(\nabla^2)$  in order to have second order derivatives that allow the use of boundary conditions such as (24). Two ways to derive this transformation will be shown in the next two subsections.

### 3.2 Substituting the mixed derivatives by the use of mass conservation

The operator  $(\nabla\nabla\cdot)$  operates on the stream function vector  $\Psi$  and gives mixed derivatives.

$$\nabla(\nabla \cdot \Psi) = \begin{pmatrix} \Psi_{xx}^I + \Psi_{xy}^{II} \\ \Psi_{xy}^I + \Psi_{yy}^{II} \end{pmatrix}, \quad \Psi = \begin{pmatrix} \Psi^I \\ \Psi^{II} \end{pmatrix}. \quad (26)$$

From the definition of  $\Psi$ , equation (1) and the Leibnitz rule of differentiation of integrals, a relation between the mixed derivative of the stream function on the undisturbed surface and the second order derivatives in  $x$  and in  $y$  can be constructed. Let us derive the Laplace operator of  $\Psi$ :

$$\begin{aligned} [\Psi_{zz}^I + \nabla^2 \Psi^I]_{z=0} &= \int_{-h}^0 u_{zz} dz + \nabla^2 \left( \int_{-h}^0 u dz \right) = \\ &= \int_{-h}^0 (u_{zz} + \nabla^2 u) dz + [(\nabla^2 h) u + 2\nabla h \cdot \nabla u - (\nabla h \cdot \nabla h) u]_{z=-h}. \end{aligned} \quad (27)$$

Here,  $\nabla^2 = \partial_x^2 + \partial_y^2$ . The horizontal velocity  $u$  satisfies the Laplace equation, as can easily be shown by taking the  $x$ -derivative of the Laplace equation of  $\Phi$ , that represents the differential conservation of mass.  $u$  on the bottom ( $z = -h$ ) can be now represented using the stream function approximation given in equation (9). Applying both relations to equation (27) and using equation (4) yields the relation

$$\partial_x \partial_y \Psi_0^{II} = \partial_y^2 \Psi_0^I - [(\nabla^2 h) \partial_z f + 2(\nabla h \cdot \nabla h) \partial_z \partial_h f]_{z=-h} \Psi_0^I. \quad (28)$$

In the same manner the mixed derivative of  $\Psi_0^I$  can be constructed,

$$\partial_x \partial_y \Psi_0^I = \partial_x^2 \Psi_0^{II} - [(\nabla^2 h) \partial_z f + 2(\nabla h \cdot \nabla h) \partial_z \partial_h f]_{z=-h} \Psi_0^{II}. \quad (29)$$

And in the vector form

$$\nabla(\nabla \cdot \Psi_0) = \nabla^2 \Psi_0 - \left[ (\nabla^2 h) \partial_z f + 2(\nabla h \cdot \nabla h) \partial_z \partial_h f \right]_{z=-h} \Psi_0, \quad (30)$$

we can see that the grad-div operator is equal to the Laplacian operator with a correction for non-flat bathymetry. The coefficients given in terms of the vertical profile  $f$  in equations (28), (29) and (30) are

$$\partial_z \partial_h f|_{z=-h} = \frac{k(h) (k(h) + k'(h)h)}{\sinh(k(h)h)} (k'(h) - \coth(k(h)h)), \quad (31)$$

$$\partial_z f|_{z=-h} = \frac{k(h)}{\sinh(k(h)h)}. \quad (32)$$

Kim & Bai [7] showed that prior to applying the vertical profile approximation, the linear equations of motion using the  $\psi$  representation satisfy both the continuity equation and the irrotational condition. Nevertheless, after applying the approximated vertical profile the situation changes. By inspecting equation (30), we can see that for the 2D problem, where  $\Psi = (\psi, 0)$ ,  $\psi$  does not satisfy Laplace's equations thus, the 3D case does not degenerate to the 2D case. It has a correction term that relates to the bottom slope and curvature. In order to coincide with the 2D case, the mixed derivatives should be substituted using a different relation.

### 3.3 Substituting the mixed derivatives by the use of irrotationality

Let us derive the Laplace operator of  $\Psi$  using the horizontal irrotational condition given in (23). Taking its  $x$  and  $y$  derivatives, the mixed derivatives of  $\Psi_0^I$  and  $\Psi_0^{II}$  can be constructed respectively to yield

$$\begin{aligned} \partial_x \partial_y \Psi_0^I &= \partial_x^2 \Psi_0^{II} + (h_y \partial_x \Psi_0^I - h_x \partial_x \Psi_0^{II}) \partial_z f|_{z=-h} - \\ &- \left[ (h_{xy} \Psi_0^I - h_{xx} \Psi_0^{II}) \partial_z f + (h_y \Psi_0^I - h_x \Psi_0^{II}) h_x \partial_z \partial_h f \right]_{z=-h}, \end{aligned} \quad (33)$$

$$\begin{aligned} \partial_x \partial_y \Psi_0^{II} &= \partial_y^2 \Psi_0^I - (h_y \partial_y \Psi_0^I - h_x \partial_y \Psi_0^{II}) \partial_z f|_{z=-h} - \\ &- \left[ (h_{yy} \Psi_0^I - h_{xy} \Psi_0^{II}) \partial_z f + (h_y \Psi_0^I - h_x \Psi_0^{II}) h_y \partial_z \partial_h f \right]_{z=-h}. \end{aligned} \quad (34)$$

where,

$$\partial_z \partial_h f|_{z=-h} = \frac{k(h) (k(h) + k'(h)h)}{\sinh(k(h)h)} (k'(h) - \coth(k(h)h)), \quad (35)$$

$$\partial_z f|_{z=-h} = \frac{k(h)}{\sinh(k(h)h)}. \quad (36)$$

And in the vector form

$$\nabla(\nabla \cdot \Psi_0) = \nabla^2 \Psi_0 + \mathbf{F}(f, h, \Psi_0), \quad (37)$$

where the vector function  $\mathbf{F}$  is defined using equations (33) and (34).

#### 4 A Parabolic approximation for the CMSE

For various problems, where the reflected waves can be neglected, it is plausible to assume a progressive wave field to the first order. The wave amplitude can contain the smaller deviations from the first order wave field. The resulting equation becomes parabolic instead of elliptic. This enables to extensively reduce the computer storage and CPU time needed for the numerical solution as the wave flow problem can be solved as a moving front. There are various ways of applying parabolic approximations. In this section a parabolic approximation will be formulated for the CMSE following a method used by Kaihatu & Kirby [11].

Let us assume the problem to have the form of a progressive wave field, so the stream function has the behavior of the following form:

$$\Psi_0 = \mathbf{A}(x, y) e^{i \int k(x, y) dx}, \quad \mathbf{A} = \begin{pmatrix} A^I \\ A^{II} \end{pmatrix}. \quad (38)$$

Here,  $A$  is a complex vector slowly varying in  $x$  and  $y$  that represents the stream function complex amplitude. Applying equation (38) to the building blocks of equation (17) yields the relations:

$$\begin{aligned} \nabla \cdot \Psi_0 &= \left( A_x^I + ikA^I \right) e^{i \int k(x, y) dx} + \left( A^{II} e^{i \int k(x, y) dx} \right)_y \\ \nabla h \cdot \Psi_0 &= h_x A^I e^{i \int k(x, y) dx} + h_y A^{II} e^{i \int k(x, y) dx} \\ \nabla(\nabla \cdot \Psi_0) &= \left( \left( A_{xx}^I + 2ikA_x^I - k^2 A^I \right) e^{i \int k(x, y) dx} + \left( \left( A_x^{II} + ikA^{II} \right) e^{i \int k(x, y) dx} \right)_y \right) \\ &\quad + \left( \left( A_x^I + ikA^I \right) e^{i \int k(x, y) dx} \right)_y + \left( A^{II} e^{i \int k(x, y) dx} \right)_{yy} \\ \nabla(\nabla h \cdot \Psi_0) &= \left( \left( h_{xx} A^I + h_x ikA^I + h_x A_x^I + h_{xy} A^{II} + h_y ikA^{II} + h_y A_x^{II} \right) e^{i \int k(x, y) dx} \right) \\ &\quad + \left( h_{xy} A^I + h_{yy} A^{II} \right) e^{i \int k(x, y) dx} + h_x \left( A^I e^{i \int k(x, y) dx} \right)_y + h_y \left( A^{II} e^{i \int k(x, y) dx} \right)_y \end{aligned}$$

$$\nabla^2 \Psi_0 = \left( \mathbf{A}_{xx} + 2ik\mathbf{A}_x - k^2\mathbf{A} \right) e^{i\int k(x,y)dx} + \left( \mathbf{A} e^{i\int k(x,y)dx} \right)_{yy} \quad (39)$$

The wave is assumed to be propagating mostly along the positive  $x$ -axis and not in the  $y$ -direction. It consists of rapid variation accounted for by the complex exponential given in equation (38). We scale the derivatives of  $A$  as follows

$$\begin{aligned} \frac{\partial A^I}{\partial x} &= O(\epsilon^2), \quad \frac{\partial A^{II}}{\partial x} = O(\epsilon^2), \\ \frac{\partial A^I}{\partial y} &= O(\epsilon), \quad \frac{\partial A^{II}}{\partial y} = O(\epsilon). \end{aligned} \quad (40)$$

Assuming that the behavior in the  $x$ -direction is mostly accounted for by the complex exponential, and by applying the ordering stated in (40), we can neglect the higher order terms  $\frac{\partial^2 A^I}{\partial x^2}$  and  $\frac{\partial^2 A^{II}}{\partial x^2}$ , which changes the equation's nature from elliptic to parabolic. In addition, the dependence of  $k$  in the  $y$ -direction should be factored out, since we integrate it only in  $x$ . Following Lozano & Liu [12], we will define a  $y$ -averaged wave number function  $\bar{k}(x)$  as a reference, so we can rewrite (38) as

$$\Psi_0 = \alpha(x, y) e^{i\int \bar{k}(x)dx}, \quad \alpha = \begin{pmatrix} \alpha^I \\ \alpha^{II} \end{pmatrix}, \quad (41)$$

which together with equation (38) gives the relation

$$\mathbf{A}(x, y) = \alpha(x, y) e^{i(\int \bar{k}(x)dx - \int k(x,y)dx)}. \quad (42)$$

Substituting equation (42) to the relations stated in (39) yields,

$$\begin{aligned} \nabla \cdot \Psi_0 &= \left( \alpha_x^I + i\bar{k}\alpha^I + \alpha_y^{II} \right) e^{i\int \bar{k}(x)dx}, \\ \nabla h \cdot \Psi_0 &= \left( h_x \alpha^I + h_y \alpha^{II} \right) e^{i\int \bar{k}(x)dx}, \\ \nabla (\nabla \cdot \Psi_0) &= \begin{pmatrix} 2ik\alpha_x^I - 2k(\bar{k} - k)\alpha^I - k^2\alpha^I + \alpha_{xy}^{II} + i\bar{k}\alpha_y^{II} \\ \alpha_{xy}^I + i\bar{k}\alpha_y^I + \alpha_{yy}^{II} \end{pmatrix} e^{i\int \bar{k}(x)dx}, \\ \nabla (\nabla h \cdot \Psi_0) &= \begin{pmatrix} h_{xx}\alpha^I + h_x i\bar{k}\alpha^I + h_x \alpha_x^I + h_{xy}\alpha^{II} + h_y i\bar{k}\alpha^{II} + h_y \alpha_x^{II} \\ h_{xy}\alpha^I + h_{yy}\alpha^{II} + h_x \alpha_y^I + h_y \alpha_y^{II} \end{pmatrix} e^{i\int \bar{k}(x)dx}, \\ \nabla^2 \Psi_0 &= \left( 2ik\alpha_x^I - 2k(\bar{k} - k)\alpha^I - k^2\alpha^I + \alpha_{yy}^{II} \right) e^{i\int \bar{k}(x)dx}. \end{aligned} \quad (43)$$

For a smooth bathymetry the CMSE (17) can be written as

$$a\nabla(\nabla\cdot\Psi_0) + ak^2\Psi_0 + b\nabla(\nabla h\cdot\Psi_0) + (b\nabla\cdot\Psi_0 + (b_h - c)\nabla h\cdot\Psi_0)\nabla h = 0. (44)$$

Together with the relations given in (43), a parabolic formulation to the CMSE is given. In order to take out the mixed derivatives, equations (33) and (34) can be used to replace the operator  $\nabla\nabla\cdot$  by  $\nabla^2$ .

## 5 Numerical Results

In this section, the CMSE and its parabolic approximation are being numerically solved in comparison with other models and laboratory experiments. The MATHEMATICA 6 software function NDSolve is used for the numerical solutions. In subsections 5.1, 5.2 and , the class I and class II reflected Bragg resonance numerical experiments and the oblique wave incidence on a plane beach were conducted as initial value problems starting from the end side backwards. In subsection 5.4 the parabolic approximation shown in section 4 was applied to allow, as before, solving the problem as an initial value one.

### 5.1 Class I Bragg resonance - oblique incidence

Class I Bragg resonance is caused by a linear interaction between one wave component and one undulating bottom components. This type of resonance has a significant effect on linear waves. The CMSE was shown to give excellent prediction for the reflection coefficient resulting of this resonance [7] in the 2D case. The problem of obliquely incident waves propagating towards an undulating bathymetry patch is a quasi-3D problem. If we set the coordinate system so that the bottom changes only in the  $x$ -direction, the wave component does not change its wave number in the  $y$ -direction and the streamfunction can be written as

$$\Psi(x, y) = \psi(x)e^{ik_y y}. (45)$$

Applying (45) to (17), yields a 1D differential equation for this problem. We used it in order to show the 2 cases of oblique incidence for class I Bragg resonance, using the same parameters as in two of the cases given by Kim & Bai [7] for the non-oblique class I Bragg resonance. The results are shown in Figure 1. Note, that the peak location of the resonance has a small shift relative to the expected  $k = \frac{1}{2}k_b$  location. The small shift given by the CMSE was shown to be accurate in comparison to the exact linear theory solution unlike the ones

of the MSE and MMSE [7]. The bottom undulation in these calculation is of wave number ratio of  $k_b h_0 = \frac{2\pi}{6.4}$  with a sinusoidal wave patch of 4 wavelengths. Figures 1a and 1c present the maximal reflection coefficients with respect to the incidence angle for the cases of  $\Delta H/H_0 = 0.32$  and  $\Delta H/H_0 = 0.64$  respectively. The results presented in Figure 1 take into account the shift of the resonance peak. Figures 1b and 1d represent the full reflection graph of Figures 1a and 1c for the same cases with respect to the frequency of the incident wave at an incidence angle of  $40^\circ$  ( $\approx 0.7\text{rad}$ ). We can see that the CMSE and MMSE give quite similar results near the class I Bragg resonance conditions. This is not surprising as both are approximated in a way that should give good results near the class I Bragg resonance conditions. Nevertheless, they behave differently away from the class I Bragg resonance.

Liu & Yue [13] have developed a high-order spectral (HOS) method and used it to solve for class I Bragg resonance in the case of oblique incidence as well. The bottom undulation was taken as  $\Delta H/H_0 = 0.16$ , the wave steepness as  $ka = 0.05$  and the undulation steepness as  $k_b \Delta H = 0.31$ . The results of the HOS method the CMSE and the MMSE are presented in Figure 1. The results of both the CMSE and the MMSE give excellent agreement to the ones of the HOS numerical model. In this case, the bottom undulation is not steep enough to cause a significant difference between the results of the CMSE to the ones of the MMSE in the class I Bragg resonance case.

## 5.2 Class II Bragg resonance

Class II Bragg resonance is caused by a linear interaction between one wave component and two undulated bottom components. This type of resonance has a minor effect on linear waves compared to class I Bragg resonance, but still can have significant effects even for small bottom undulation components, see Guazzelli, *et al.* [14]. Kim & Bai [7] presented the CMSE numerical calculations for class I Bragg resonance. These calculations also apply for class II Bragg resonance in the case where the incident wave's wavenumber equals the bottom undulation's wavenumber. In this unique case, the solution presented a good behavior in the class II Bragg region as well. Here, the CMSE is solved in comparison to laboratory experiments of Guazzelli, *et al.* [14] with doubly periodic bottom undulations. The results in Figure 3, show that the CMSE as the MMSE and as other MS-type equations is not able to accurately model this type of phenomenon. This is a common inaccuracy of MS-type equations, as within the mechanism of the class II Bragg resonance a bottom induced wave plays a major role. This wave has a vertical velocity structure, which has a different wave number than the one of the incident wave assumed in MS-type equations, and that leads to significant errors.

### 5.3 *Oblique wave incidence on a plane beach*

The problem of obliquely incident waves propagating towards a sloped beach is, as well, a quasi-3D problem. Again, as in subsection 5.1, the 1D differential equation developed by applying (45) to (17) was used to solve this problem. The results for the numerical experiment of the CMSE and the MMSE together with an accurate analytical solution of Ehrenmark [15] are given in Figure 4. We can see that both the CMSE and the MMSE show good agreements with an advantage to the ones of the CMSE.

### 5.4 *Submerged two-dimensional obstacle*

Ito & Tanimoto [16] conducted a wave tank experiment of monochromatic waves propagating on a flat bottom with a circular shoal area. The chopped sphere underwater sea mount acts as a lens that focuses the waves and creates a cusped caustic. For this type of problems, where geometrical ray methods fail, the MS-type models are plausible to use. The bathymetry and the monitored sections are shown in Figure 5. The constant bottom depth surrounding the shoal is  $h_0 = 0.15m$ . The center of the circular shoal area is located at  $(x_c, y_c) = (1.2, 1.2)$  giving the shallowest water depth as  $0.05m$ . The water depth at the shoal area ( $r \leq 0.8m$ ) is defined as

$$h(x, y) = 0.05 + 0.15625m^{-1} \left( (x - x_c)^2 + (y - y_c)^2 \right).$$

The wave height was given by  $H = 1.04cm$  and the period by  $T = 0.511sec$ .

The linear parabolic CMSE model given in equation (17) and the parabolic definitions set (43) were used for the numerical run. The mixed derivatives were substituted using equations (33) and (34). The boundary conditions at the impermeable walls ( $y = 0$  and  $y = 2.4$ ) were given as  $\Psi^{II} = 0$ , which indicates a zero velocity toward the wall, and  $\Psi_y^I = 0$ , which is the outcome of the irrotationality condition on the wall given by equation (23). The results for the numerical experiment together with the wave-tank ones are given in Figure 6, and show very good agreements. Note that the results of Ito & Tanimoto[16] fail to be symmetric as is expected due to the symmetry of the experiment's set-up. Therefore, the wave gauge measurements in transections 2 and 3, which are given in Figure 6, are duplicated as a mirror image in order to present the results in a symmetric way.

## 6 Summary and conclusions

In the present work, the Complementary-Mild Slope Equation was re-derived using the Irrotational Green-Naghdi Lagrangian with a correction for the 3D case. The difficulties in solving this equation in the 3D case were presented and accounted for using the irrotationality condition. This allows to exploit the superior accuracy of the CMSE model in 3D water wave problems as well. In addition, a parabolic approximation is applied to the CMSE in order to construct a simpler model, which is applicable to wave problems with insignificant reflection.

The corrected CMSE model is solved in comparison with an accurate numerical model, an accurate analytical solution and a wave tank experiment of 3D nature. The results show very good agreements, and extends the use of this model for practical engineering problems of 3D nature.

## Acknowledgments

This research was supported by the US-Israel Binational Science Foundation (Grant 2004-205) and by the Germany-Israel (BMBF-MOST) Joint Research program (Grant 1946).

## References

- [1] J. C. W. Berkhoff, Computation of combined refraction-diffraction, Proc. of the 13th Int. Conf. on Coastal Engineering ASCE (1972) 471–490.
- [2] T. W. Hsu, T. Y. Lin, C. C. Wen, S. H. Ou, A complementary mild-slope equation derived using higher-order depth function for waves obliquely propagating on sloping bottom, Phys. of Fluids. 18 (8) (2006) 087106.1–14.
- [3] S. R. Massel, Extended refraction-diffraction equation for surface waves, Coastal Eng.. 19 (1993) 97–126.
- [4] P. G. Chamberlain, D. Porters, The modified mild slope equation, J. Fluid Mech. 291 (1995) 333–407.
- [5] J. T. Kirby, A general wave equation for waves over rippled beds, J. Fluid Mech. 162 (1986) 171–186.
- [6] Y. Agnon, Linear and nonlinear refraction and bragg scattering of water waves, Phys. Rev. E 59 (1999) 1319–1322.

- [7] J. W. Kim, K. J. Bai, A new complementary mild-slope equation, *J. Fluid Mech.* 511 (2004) 25–40.
- [8] A. E. Green, P. M. Naghdi, Oblique wave incidence on a plane beach: the classical problem revisited, *Proc. R. Soc. London A* 347 (1976) 447–473.
- [9] J. W. Kim, K. J. Bai, R. C. Ertekin, W. C. Webster, A derivation of the green-naghdi equations for irrotational flows, *J. of Eng. Math.* 40 (2001) 17–42.
- [10] J. W. Kim, K. J. Bai, R. C. Ertekin, W. C. Webster, Water waves in water of variable depth - the irrotational green-naghdi model, *J. of Offshore Mech. and Arctic Eng.* 125 (2003) 25–32.
- [11] J. M. Kaihatu, J. T. Kirby, Nonlinear transformation of waves in finite water depth, *phys. Fluids* 8 (1995) 175–188.
- [12] C. J. Lozano, P. L. F. Liu, Refraction-diffraction model for linear surface water waves, *J. Fluid Mech.* 101 (1980) 705–720.
- [13] Y. Liu, D. K. P. Yue, On generalized bragg scattering of surface waves by bottom ripples, *J. Fluid Mech.* 356 (1998) 297–326.
- [14] E. Guazzelli, V. Rey, M. Belzons, Higher-order bragg reflection of gravity surface waves by periodic beds, *J. Fluid Mech.* 245 (1992) 301–317.
- [15] U. T. Ehrenmark, Oblique wave incidence on a plane beach: the classical problem revisited, *J. Fluid Mech.* 368 (1998) 291–319.
- [16] Y. Ito, K. Tanimoto, A method of numerical analysis of wave propagation: Application to wave diffraction and refraction, *Proc. 13th Int. Conf. Coastal Eng. ASCE* 291 (1972) 503–522.

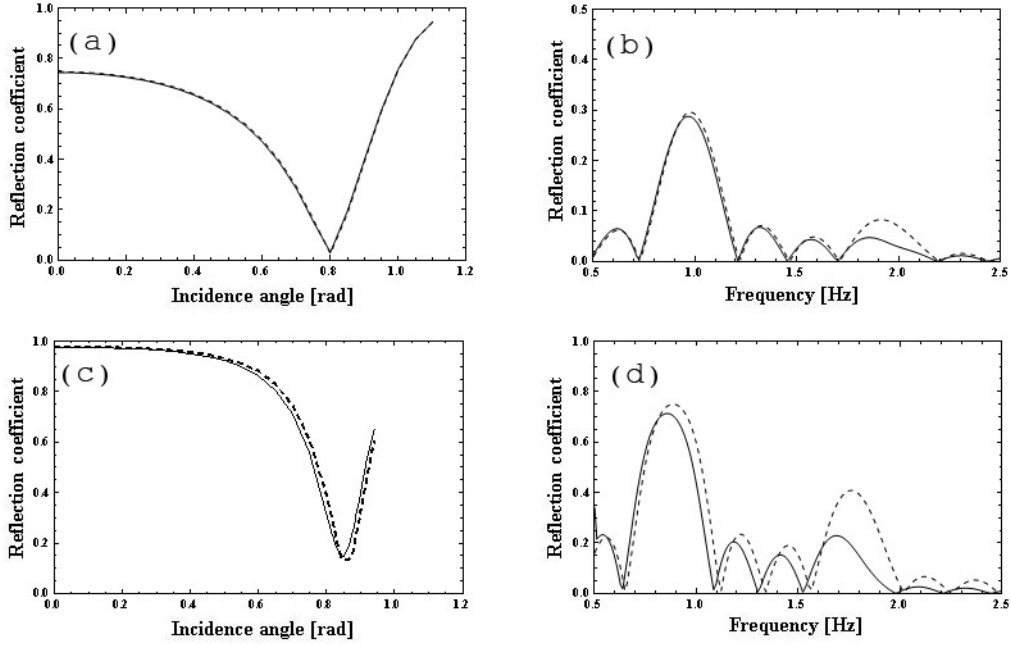


Figure 1. The reflection coefficients of the CMSE (solid) and the MMSE (dot-dashed) for oblique incidence class I Bragg resonance reflection. Figure (a): the maximal reflection coefficient with respect to the incidence angle for  $\Delta H/H_0 = 0.32$ . Figure (b): the reflection coefficient for a single angle of  $40^\circ$  for  $\Delta H/H_0 = 0.32$ . Figure (c): the same as Figure (a) for  $\Delta H/H_0 = 0.64$ . Figure (d): the same as Figure (b) for  $\Delta H/H_0 = 0.64$ .

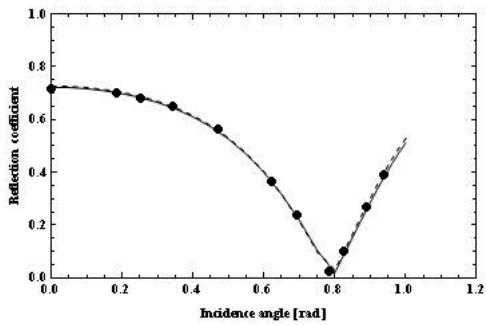


Figure 2. The reflection coefficients of the CMSE (solid) and the MMSE (dot-dashed) for oblique incidence class I Bragg resonance reflection with respect to numerical results of Liu & Yue [13] (dotted) for  $\Delta H/H_0 = 0.16$ .

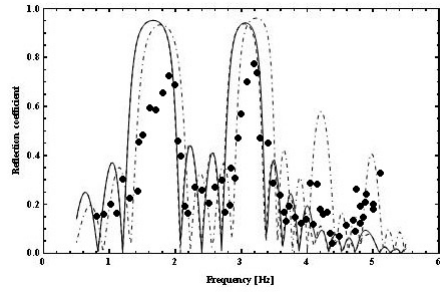


Figure 3. The reflection coefficients of the CMSE (solid), the MMSE (dot-dashed) and the laboratory experiment measurements of Guazzelli, *et al.* [14] (solid circles) for the case of sea bed with  $K_1 = 0.52\text{cm}^{-1}$  and  $K_2 = 1.05\text{cm}^{-1}$ , patch length of  $L = 48\text{cm}$  and amplitude ratios of  $\Delta H/H_0 = 0.4$  and mean water depth of  $H_0 = 2.5\text{cm}$ .

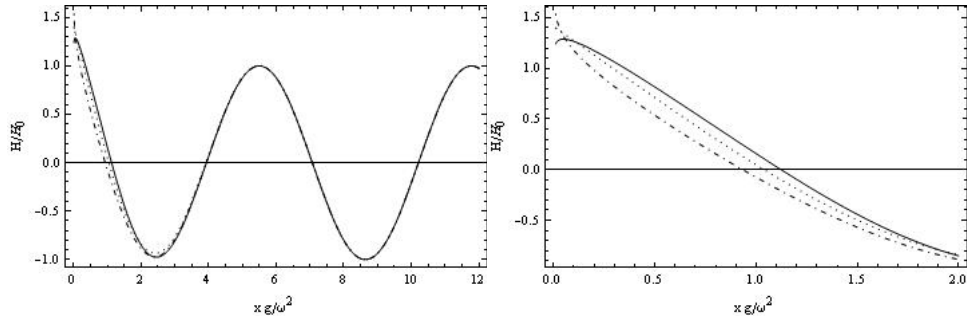


Figure 4. The normalized wave height of the CMSE (solid) and the MMSE (dot-dashed) with respect to the analytical solution of Ehrenmark [15] (dotted) for a  $45^\circ$  incidence angle wave on a  $45^\circ$  plane beach.

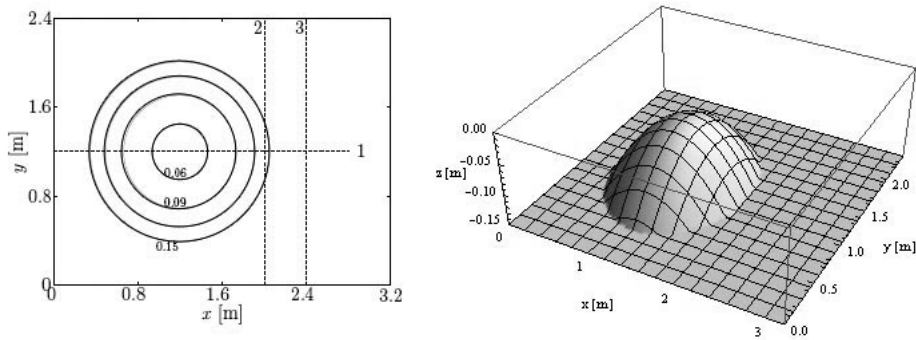


Figure 5. The bathymetry in the experiment of Ito & Tanimoto [16]. The wave maker is positioned at  $x = 0$ . Dashed lines indicate the transections monitored by wave gauges. All units are stated in meters.

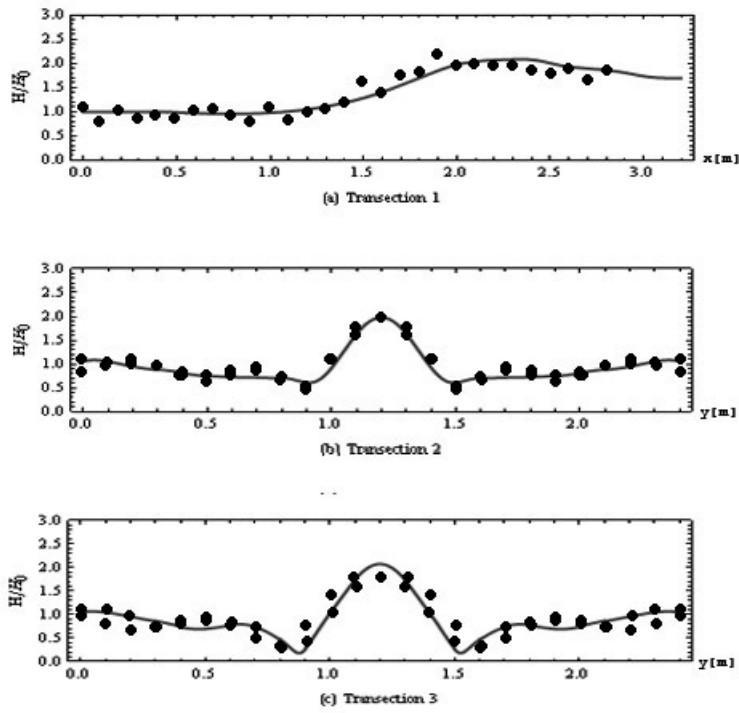


Figure 6. The normalized wave height for the experiment of Ito & Tanimoto [16]. The numerical results of the CMSE (solid) are given together with the wave gauge measurements (solid circles). The wave height was given as  $H = 1.04\text{cm}$  and the period as  $T = 0.511\text{sec}$ . The location of the transections are given in Figure 5.

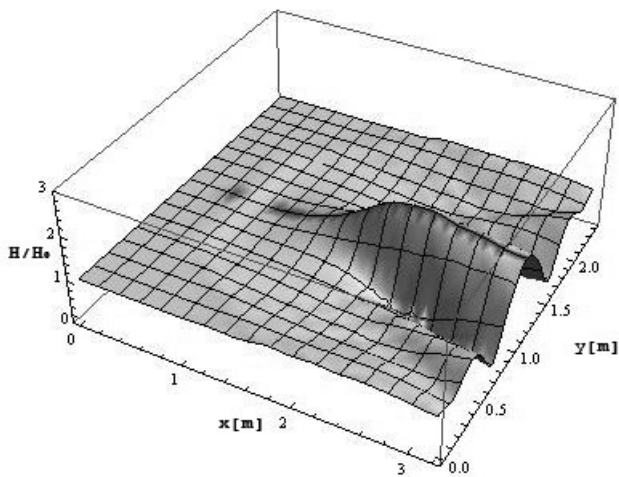


Figure 7. The normalized wave height numerical results of the CMSE for the experiment of Ito & Tanimoto [16]. The wavemaker is positioned at  $x = 0$ .